Identifying physical properties of a CO_2 laser by dynamical modeling of measured time series

W. Horbelt and J. Timmer*
Fakultät für Physik, Albert-Ludwigs-Universität, Hermann-Herder-Strasse 3, D-79104 Freiburg, Germany

M. J. Bünner
EPCOS AG, Anzinger Strasse 13, 81617 München, Germany

R. Meucci and M. Ciofini
Istituto Nazionale di Ottica Applicata, Largo Enrico Fermi 6, 50125 Firenze, Italy

(Received 13 November 2000; revised manuscript received 2 April 2001; published 26 June 2001)

We estimate internal parameters of a *Q*-switched CO_2 laser by fitting trajectories of the four-level model to measured scalar time series. The four-level model is a five-dimensional nonlinear system of ordinary differential equations. A multiple shooting technique is used to construct the unobserved time courses of the population densities and to reveal the dependence of the parameters on the excitation current. For excitations barely above the laser threshold large pulse variations are identified as an effect of small variations of the pump parameter.

DOI: 10.1103/PhysRevE.64.016222 PACS number(s): 05.45.Tp, 42.55.Lt, 42.60.Gd, 42.65.Sf

I. INTRODUCTION

Experimentally observed dynamical systems are frequently modeled in terms of nonlinear ordinary differential equations (ODE). Typically, not all relevant internal variables and parameters of a system are easily accessible to direct measurements. The deterministic ODE defining the system contains unknown parameters and unobserved components. In the case of nonlinear ODEs, Fourier analysis is not applicable and analytic solutions are not available in general.

Sometimes educated guesses are made for the parameters and the resulting model trajectories are compared with measured data by visual inspection [1–6]. In absence of a systematic adaptation of the mathematical models, it cannot be distinguished between discrepancies that stem from wrongly chosen parameters in a sufficient model on the one hand and shortcomings of the model itself on the other. A fair comparison between two different model classes requires that the models be optimized with respect to their parameters first.

Other approaches make use of Taken's embedding theorems [7]. *Time delay embedding* [8–10] works with phase spaces and parameters, which typically do not have a physical interpretation. In the case of *differential embedding* [6,11,12], time derivatives must be estimated from the data, severely amplifying the measurement noise. Furthermore both embedding techniques raise the so-called errors-in-variables problem. It implies that estimated parameters are biased in presence of observational noise if the estimation problem is simply converted into a regression problem [13,14].

In this paper we take into account the information about the deterministic nature of the underlying true trajectory, i.e., we find the model trajectory that satisfies the ODE and comes closest to the observed data in terms of an appropriately defined cost function. The difficulty is to find the global minimum of the cost function. Since the solution of an ODE is rather sensitive to the parameters, there will usually exist numerous local minima apart from the global one. This problem is overcome by the *multiple shooting method* introduced in [15] and, in a more general context, by Bock [16].

This approach is feasible if a parametric ODE model is on hand. Regarding the *Q*-switched CO_2 laser, the so-called four-level model (4LM) is well established [17,18]. It is a nonlinear, five-variable ODE with six unknown parameters that shall be estimated from the univariate, time-resolved measurement of the intensity of a *Q*-switched CO_2 laser.

This paper is organized as follows: In Sec. II the methods for estimating parameters in differential equations are outlined and adapted to the *Q*-switched CO_2 laser. Section III shows in a simulation study that the application of the methods yields reliable estimates of the parameters under realistic conditions. The results for measured time series are reported in Sec. IV.

II. METHODS

A. Notations

Consider a time-continuous, dynamical process described by *m* nonlinear ordinary differential equations

$$\dot{\mathbf{x}} = \mathbf{f}(t, \mathbf{x}, \mathbf{p}), \quad \mathbf{x} \in \mathbf{R}^m, \quad t \in [0, T], \tag{1}$$

with a set of unknown parameters $\mathbf{p} \in \mathbf{R}$. The initial values $\mathbf{x}(0)$ are included in $\mathbf{p}$ as additional parameters. The scalar time series $\{y_i\}$ represents a noisy measurement of the dynamical variables via the observation function *g*,

$$y_i = g(\mathbf{x}(t_i, \mathbf{p}), \mathbf{p}) + \eta_i, \quad i = 1, \ldots, N, \tag{2}$$

where η_i denotes independent normally distributed random numbers with zero mean and variance σ_i^2.

*Corresponding author. Email address: jeti@fdm.uni-freiburg.de

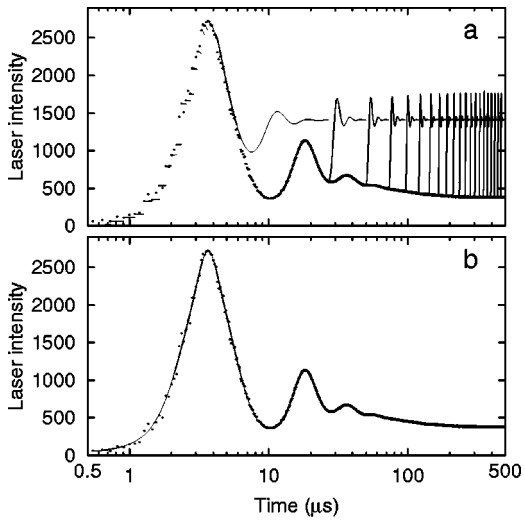

FIG. 1. Iterative fit process for a simulated time series corresponding to $i=4.80$ mA. Dots, data; lines, model trajectory. The time axis is logarithmic in order to make the first peak more distinct. (a) Initial guess: in the rear part the initial values of the multiple shooting subintervals do not yet ''know'' that the Q-switch is already past. (b) Convergence after 23 iterations.

The aim is to find those parameters $\hat{\mathbf{p}}$, for which the solution $\hat{\mathbf{x}}(t,\hat{\mathbf{p}})$ of Eq. (1) is closest to the observed dynamics. To this end, the objective function

$$\chi^2(\mathbf{p})=\sum_{i=1}^{N}\left(\frac{y_i-g(\hat{x}(t_i,\mathbf{p}),\mathbf{p})}{\sigma_i}\right)^2 \tag{3}$$

is minimized with respect to $\mathbf{p}$. Under the given assumptions one yields the *maximum-likelihood estimator* of the true parameters.

This nonlinear optimization problem is solved with a generalized Gauss-Newton method. The derivatives of the trajectory with respect to initial values and parameters are computed by integrating the *variational equations* of the ODE [19]. Since $\chi^2(\mathbf{p})$ has a highly nonlinear dependence on $\mathbf{p}$, it will usually have numerous local minima apart from the global one that corresponds to the best choice of the parameters. This problem is addressed by using the multiple shooting method.

Details of its mathematical and implementational aspects are given in [16]. An exemplification of the method is given in Sec. III. A comprehensive description of the application to the CO_2 laser is part of a forthcoming PhD thesis [20].

B. Experimental setup

The experimental setup (Fig. 2) consists of a single-mode CO_2 laser with an intracavity electro-optic modulator (EOM) [21]. The optical cavity, 1.35 m long, is defined by an 80% reflectivity spherical mirror (radius of curvature 3.0 m) and by a grating blazed for 10.6 μm. The mirror, acting as the cavity out coupler, is mounted on a piezoelectric translator in order to control the tuning between the cavity mode and the center of the molecular line. The active medium, a gas mixture of 14% CO_2, 14% N_2, 2% H_2, and 70% He at an average pressure of 21 Torr, is contained in a pyrex tube terminated by Brewster windows. The medium is excited by a high voltage DC discharge current stabilized to better than 0.01 mA.

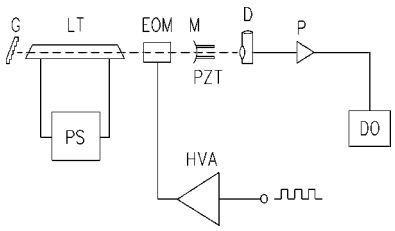

FIG. 2. Experimental setup: G, grating; LT, laser tube; EOM, electro-optic modulator; M, spherical mirror; PZT, piezoelectric translator; PS, current stabilized power supply; HVA, high-voltage amplifier; D, detector; P, preamplifier; DO, digital oscilloscope.

At 6 ms intervals the EOM driver provides 600-V pulses of 3 ms duration with rise time shorter than 50 ns. At the switch on at time $t=0$, a fast jump of the cavity-loss rate K from a higher value K_1 to a lower value K_2 is induced. $K_2=1.37$ MHz was used in all cases. This kind of (steep) external modulation induces the laser to explore both the linear and the nonlinear regimes of amplification. The laser intensity is detected with a Hg-Cd-Te photodiode and then amplified.

The detecting device has a weak nonlinearity and a bandwidth of approximately 400 kHz. The parameters of these properties were determined by an additional calibration procedure. While the nonlinearity was directly built into the observation function g in Eq. (2), the low-pass characteristic was compensated by correcting the measured data. These steps are discussed comprehensively in [20].

When the laser net gain is positive, the intensity describes a large spike, followed by relaxation oscillations. At the end of the EOM pulse, K jumps back to K_1 for another 3 ms before the next Q switch is induced. In [22] the time interval to reach thermal equilibrium was directly measured to be of the order of 3 ms for a voltage-stabilized power supply. In our experiment the power supply is highly stabilized for current fluctuations as those occurring during the Q switch. Taking this into account, a 3-ms break is a sufficient time interval to reach thermal equilibrium and then to switch on the laser again.

As the peak intensity depends on the value of the population inversion that is proportional to the discharge current, we choose the discharge current i as the control parameter, recording a sequence of 10–11 Q-switch events for different current values between 4.20 and 5.22 mA. By increasing the current a growth of the pulse height is observed, accompanied with a reduction of the delay time between the EOM pulse and the laser pulse [3].

C. Dynamical models

As a model for the dynamics of the CO_2 laser we use the five-dimensional 4LM as described in [3]. A schematic diagram of the model is shown in Fig. 3. It includes two resonant levels whose populations are denoted by N_1 and N_2,

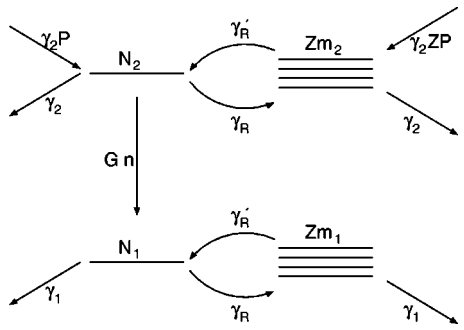

FIG. 3. Schematic diagram of the four-level model after [3].

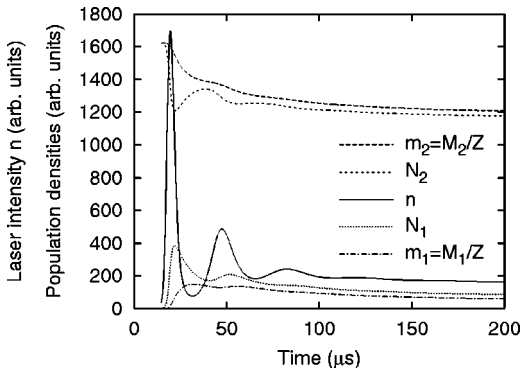

FIG. 4. Constructed time series of observed and unobserved components of the state vector for $i=4.40$ mA. The laser intensity n exhibits a large spike followed by relaxation oscillations to a steady level. The oscillations are reflected in the densities of the lasing levels N_i while they are damped in the other levels of the rotational manifold.

respectively. There are Z additional rotational levels in each vibrational band with total population densities M_1 and M_2. Their average population densities $m_i=M_i/Z$ are used as dynamic variables instead of M_i, because they have the same order of magnitude as N_i, thus making the ODE integration and the optimization numerically more efficient.

The populations decay reversibly into levels of the same band with the rate constant γ_R' and irreversibly into other levels with rate constants γ_1 and γ_2, respectively. The flux from a lasing level N_i to its other rotational levels is $Z\gamma_R'N_i=:\gamma_R N_i$. The population inversion $\delta=N_2-N_1$ is achieved by a pump rate $\gamma_2 P$ acting on each upper level.

The measured laser intensity is proportional to the photon density n. It is amplified by stimulated emission with a field-matter-coupling constant G and damped with a cavity-loss parameter $K(t)$. The time constant of the Q switch is smaller than 50 ns and can be neglected in the model. K is instantaneously switched from K_1 to K_2 at time zero.

Spontaneous emission fluctuations can also be neglected. They cause only a time shift of the trajectories [3], which is accounted for in the preprocessing described below. The 4LM reads then

$$\dot{n}=[-2K(t)+G\delta]n, \tag{4a}$$

$$\dot{N}_1=-\gamma_R N_1+\gamma_R m_1+G\delta n-\gamma_1 N_1, \tag{4b}$$

$$\dot{N}_2=-\gamma_R N_2+\gamma_R m_2-G\delta n-\gamma_2 N_2+\gamma_2 P, \tag{4c}$$

$$\dot{m}_1=+\gamma_R' N_1-\gamma_R' m_1-\gamma_1 m_1, \tag{4d}$$

$$\dot{m}_2=+\gamma_R' N_2-\gamma_R' m_2-\gamma_2 m_2+\gamma_2 P, \tag{4e}$$

with

$$\gamma_R=Z\gamma_R'.$$

The laser intensity I measured by the detector is proportional to the photon density n inside the cavity,

$$I=kn. \tag{5}$$

The unknown coefficient k is eliminated by scaling n, N_i, M_i, P, and G^{-1} with k. The ODE system is invariant under this gauge transformation but one has to keep in mind that the transformed state variables and parameters contain an unknown factor.

The qualitative behavior of the model is visualized in Sec. III. It is important to observe that there is a symmetry between γ_1 and γ_2 in the model. When a solution of Eq. (1) with certain parameters is given, the transformation

$$\tilde{n}=n, \tag{6a}$$

$$(\tilde{N}_1,\tilde{N}_2)=(P-N_2,P-N_1), \tag{6b}$$

$$(\tilde{m}_1,\tilde{m}_2)=(P-m_2,P-m_1), \tag{6c}$$

$$(\tilde{\gamma}_1,\tilde{\gamma}_2)=(\gamma_2,\gamma_1), \tag{6d}$$

leads to another solution with the same observation. Thus it cannot be decided from a measurement of n, whether the first or the second solution is true. We account for this by restricting us to solutions with $\gamma_1\geqslant\gamma_2$.

D. Consistency of the initial state vector

A crucial point in the optimization process is the beginning of the fit interval. When we treated the initial values of all state variables as free parameters, the algorithm signaled rank deficiency and the estimated unobserved components were unreasonable, i.e., it was not possible to estimate all parameters and initial values simultaneously from the given data. This problem can be solved by making sure that the initial state is consistent with the past history of the data, i.e., by incorporating additional physical knowledge about the laser buildup.

1. Low and medium excitation currents

For currents not too high, the system is in a steady state before the Q switch:

$$n \simeq 0, \tag{7}$$

$$N_1 = m_1 = 0, \tag{8}$$

$$N_2 = m_2 = P. \tag{9}$$

However, if the fit started at $t=0$, the trajectory would be arbitrarily sensitive to numerical fluctuations of n's initial value n_0, rendering the problem ill posed. Therefore the fit start was placed at the time where the intensity reaches 2% of its peak value. At this time, n, N_1, and m_1 are still small and N_2, m_2, and δ can be approximated by their steady state values. Thus the ODE is reduced to the linear system $\dot{\mathbf{x}} = \mathbf{L} \cdot \mathbf{x}$ with $\mathbf{x} = (n, N_1, m_1)^T$ and $\mathbf{L}$ being a 3×3 matrix of constants depending on $\mathbf{p}$.

The region of validity of the linear system is called the linear regime. The only positive eigenvalue of $\mathbf{L}$ is the initial laser net gain $\lambda = -2K_2 + GP$. The amplitude of the Q-switch peak and the time at which it occurs are strongly dependent on λ. The corresponding eigenvector $\mathbf{v}$, defined through

$$\mathbf{L} \cdot \mathbf{v} = \lambda \cdot \mathbf{v}, \tag{10}$$

increases exponentially until the effects of the nonlinearities become significant. Accordingly, the proportions of n, N_1, and m_1 at the fit start are given by $\mathbf{v}$. Equations (9) and (10) are used to relate the initial values of the unobserved components at the fit start to n_0 via equality constraints in the optimization process [20].

2. High excitation currents

For high currents and resultingly large pump parameters, the laser gain is always positive. Consequently the laser is switched between two different on states. The threshold for this condition can easily be determined in the experiment, since it causes the disappearance of the pulse time jitter. As another consequence the data points prior to $t=0$ correspond to a steady state with nonvanishing intensity. For these currents the fit start was placed at $t=0$ and the steady state equations that result when the right hand sides of Eqs. (4b)–(4e) are set to zero were used as constraints to the initial values.

III. SIMULATION STUDY

In this section the effectiveness of the outlined methods is demonstrated under realistic conditions. A time series of the laser intensity was simulated over $T=500$ μs with a sampling frequency of 11 MHz using Eq. (4) with the parameters that were estimated in Sec. IV for the excitation current $i=4.80$ mA. Similar results were obtained for the other currents. Noise with the same properties as in the measured data was added. Then the parameters G, γ_1, γ_2, γ_R, γ_R', and P were estimated as described above. Their starting guesses have been set to twice the true values. The initial value n_0 was another free parameter while the other initial values were related to n_0 according to Sec. II D 2.

The fit converged after 23 iterations. Figure 1 shows the starting and the final iteration of the iterative process. The estimated parameters deviated by at most 4% from the true values. Figure 4 shows all five components of the model trajectory.

The ability to construct estimates of the hidden variables of the physical system is one of the advantages of our modeling procedure compared to delay embedding techniques. In this context the detection of overparametrizations by the optimization algorithm is important to preclude continuous ambiguities in the construction. However, as Eq. (6) shows, discrete ambiguities can never be precluded.

TABLE I. Overview of recorded time series.

Regime	Low currents	Medium currents	High currents
Current i	4.20	4.40	4.80
(mA)	4.30	4.50	4.90
		4.60	5.05
		4.70	5.22

IV. EXPERIMENTAL RESULTS

Ten records with different pump currents were measured and divided into three groups with respect to their dynamical behavior. Table I gives an overview. Each record contains 10 or 11 Q-switch pulses, sampled with 1 MHz resolution. For each pulse the baseline was subtracted, which was estimated by the last 500 points before the Q switch. For high currents the laser intensity is nonzero at $t=0$. Therefore the baselines determined for low and medium currents had to be averaged and substituted for the high currents. We made sure that the impact on the estimated parameters was not larger than 1%.

All records were corrected for the low pass characteristics. The nonlinearity was directly implemented as the observation equation. The preprocessed data are given as points in the following figures.

A. Low currents

As mentioned above, the amplitude of the Q-switch peak is strongly influenced by the laser net gain $\lambda = -2K_2 + GP$. P increases with the pump current and for currents below 4.20 mA no laser action can be observed at all, indicating that λ crosses zero just below $i=4.20$ mA. For low currents, GP is only slightly above $2K_2$. Small fluctuations in the pump current then cause large relative variations in the laser net gain resulting in a dynamics that differs considerably between the individual pulses as shown for the lowest current $i=4.20$ mA in Fig. 5.

This qualitative effect was already understood theoretically and confirmed experimentally [23,24]; however, no quantitative comparison between theory and experiment was made in these studies. With our approach we are able to model the measured data in full detail. In a *multiexperiment*

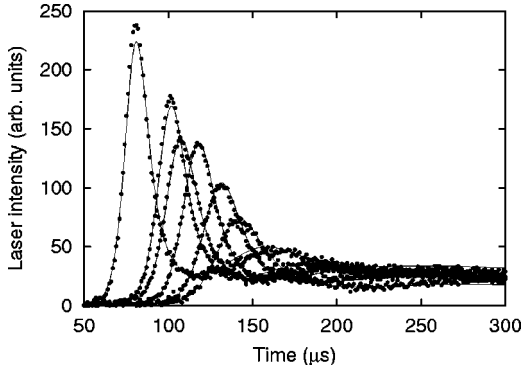

FIG. 5. Data (points) and model trajectories (lines) for the lowest pump current $i=4.20$ mA. For the sake of clarity only 6 of 11 pulses are shown. The large variability of the curves was reproduced very well although only P and n_0 were varied independently for each pulse. The estimated parameters are given in the text.

analysis all pulses were utilized simultaneously. Only the pump parameter P was allowed to attain an individual value for each pulse while G, γ_1, γ_2, γ_R, and γ_R' were forced to be the same for all pulses.

As Fig. 5 shows, both the amplitudes and shapes of all pulses are reproduced well. The estimated parameters are: $G=26.7\times10^{-12}$ s^{-1}, $\gamma_1=25.7$ kHz, $\gamma_2=4.79$ kHz, $\gamma_R=42.0$ kHz, $\gamma_R'=24.9$ kHz, $P=109\times10^{15}$.

In Fig. 6 the estimated value of P and the resulting net gain λ are plotted vs the experimental pulse height. A clear monotone functional relationship can be seen. The empirical relative standard deviation of P is only 1.4%, i.e., P does not make large use of its freedom to vary between the records. On the other hand, λ has a relative standard deviation of 22% being responsible for the broad spectrum of pulse shapes.

The good correspondence between measurements and model can be taken as a strong plea for the validity of the four-level model for this experimental condition. For $i=4.30$ mA the situation is similar but less distinct. In this case the standard deviation of P is again 1.4% while that of λ is 6.5%.

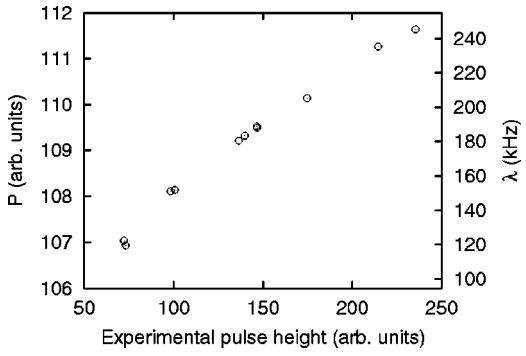

FIG. 6. Relation between the experimental pulse heights and the estimated values of P (left axis) and $\lambda=-2K_2+GP$ (right axis) for $i=4.20$ mA. Note the ranges of the two axes for P and λ. There is a factor 2 between the minimum and the maximum of λ while the P values cover a range that is only the 20th part of their mean.

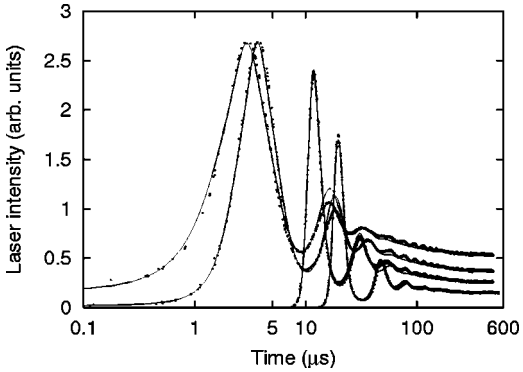

FIG. 7. Measured data (points) and best fit trajectories (lines) for a representative selection of medium and high currents. The currents shown are $i=5.22$, 4.80, 4.60, and 4.40 mA. The peaks appear from left to right in the given order, the tails from top to bottom. The other currents are omitted for the sake of clarity. The time axis is logarithmic in order to make the first peaks more distinct. For the high currents, the baseline is nonvanishing.

B. Medium and high currents

For currents $i=4.40$ mA and higher, the variance in the pulse height is strongly reduced since the variance of the net gain is small compared with its absolute value. Moreover the peak becomes narrower with increasing current, thus being sampled by successively fewer data points. In order to increase the sampling frequency, all pulses of a record are merged into a single time series. The data points are not averaged but only gathered together with time values shifted such that each pulse has time zero at a trigger point. As trigger point serves the time at which the first decline after the large peak falls below the second maximum. For medium currents the pulse shapes are not yet perfectly equal, thus the merged time series seem to contain some noise as can be seen in Fig. 7.

The procedure for estimating the laser parameters was applied to each record to estimate the parameters G, γ_1, γ_2, γ_R, γ_R', and P. Data and best fit trajectories are shown in Fig. 7. In order to emphasize the peak region, a logarithmic abscissa is used. No rank deficiency was encountered by the algorithm. The model trajectories follow the experimental data well. Especially the main peaks are reproduced well.

For high currents the second peak is slightly overestimated and the relaxation oscillations that are coherent over the complete time interval, are not resembled in detail by the model.

Figure 8 summarizes the estimated parameters for medium and high currents. The statistical errors shown in the figure are calculated from the inverse of the *Hesse matrix* of the objective function, based on the assumption that the observational noise is uncorrelated. However, due to the low pass characteristic of the detector and the pulse merging procedure, the noise has got a more complicated correlation structure. Moreover systematic errors introduced by the preprocessing and model mis-specifications are not reflected in the estimated confidence intervals. Therefore the displayed error bars should not be overinterpreted.

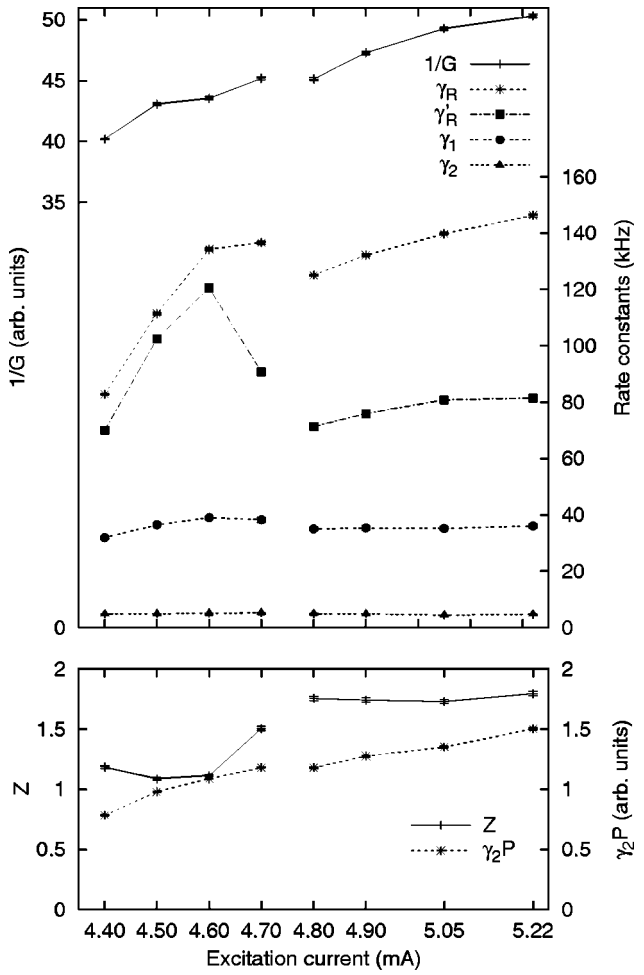

FIG. 8. Estimated parameters and error bars as a function of the excitation current for medium and high currents. From top to bottom: $1/G$ (top left axis); rate constants γ_R, γ'_R, γ_1, and γ_2 (top right axis); number of rotational levels Z (bottom left axis); pump rate $\gamma_2 P$ (bottom right axis). $1/G$ and P contain an unknown scaling factor that is, however, the same for all records. The results and error bars are discussed in the text.

For high currents the laser is enduringly above threshold as mentioned before. This qualitative difference between medium and high currents was emphasized by drawing lines between points within but not between these two groups.

The rate constants γ_1, γ_2, γ_R, and γ'_R increase with the current, which reveals their temperature dependence. γ_1 was estimated to be much larger than γ_2 in accordance with [18,5], thus the assumption $\gamma_1 = \gamma_2$ made in [25,26] is rejected based on dynamically modeled measured time series. In this context we would like to mention briefly that the application of the simpler two-level model [1,27] turned out to be insufficient to describe the given data adequately.

The field matter coupling constant G is inversely proportional to the collisional broadening $\gamma_\perp$ [27]. G decreases with increasing current. This can be understood as a temperature induced increase of $\gamma_\perp$. Therefore we plotted $1/G$ together with the rate constants and actually it shows a similar behavior.

The pump rate $\gamma_2 P$ increases monotonically with the pump current as expected. The effective number of rotational levels is not estimated directly but calculated through $Z = \gamma_R / \gamma'_R$. It increases with the current and has values between 1 and 2 in contrast to thermodynamic considerations suggesting higher values. Also, γ'_R and γ_R are considerably smaller than the values used in the literature [28,17,3,18]. As the gas mixture, its total pressure, the geometry of the discharge tube (i.e., internal diameter, electrode shapes, etc.), and the excitation currents are different, it is difficult to compare estimated parameters with values obtained by spectroscopic measurements. However, the low values estimated for Z are an indication of an intrinsic weakness of the 4LM, which is too simplified a model to represent the complex molecular dynamics in a CO_2 laser. Taking into account the four unobserved components and the coupling between their initial values and the parameters (Sec. II D), it is difficult to assess the impact of model misspecifications on the estimated parameters. Future work must be devoted to an evaluation of refined models.

The comparison between the experimental results and the outcomes of the fitting procedure remains essential. In this framework, our numerical estimations confirm the essential role played by the incoherent processes ruled by the collisional rates γ_R and γ'_R.

As a final result, the steady state condition $\dot{n} = 0$ is used to estimate the value K_1 of the cavity losses before the Q switch for high currents. The result was between 2.42 and 2.54 kHz for the four records, i.e. almost the same value was estimated independently in all four records.

V. CONCLUSION

In this paper we modeled measured time series from a Q-switched CO_2 laser on the basis of the four-level model (4LM). The unobserved dynamical variables of a five-dimensional differential equation scheme were constructed and the internal parameters were estimated. The method was tested on simulated data under realistic conditions and it was applied to ten records of measured data with differing excitation currents.

For low pump currents we could explain a large variability of the pulse shapes through rather small variations in the pump parameter. For a wide range of higher pump currents the 4LM is able to reproduce well the large main peak as well as the long tails of the relaxation phase.

Our study also confirms in an unequivocal and independent way the important role of the rotational manifolds in the dynamics of a CO_2 laser. For the first time, to the best of our knowledge, a convincing correspondence between measured time series from a CO_2 laser and model trajectories from the four-level model was obtained. We expect that this approach of investigating dynamical systems by modeling ''*in vivo*'' experiments will enable detailed insight into numerous challenging complex phenomena.

[1] F.T. Arecchi, W. Gadomski, R. Meucci, and J.A. Roversi, Opt. Commun. **65**, 47 (1988).
[2] M. Ciofini, A. Politi, and R. Meucci, Phys. Rev. A **48**, 605 (1993).
[3] R. Meucci, M. Ciofini, and P. Wang, Opt. Commun. **91**, 444 (1992).
[4] C.O. Weiss *et al.*, Appl. Phys. B: Lasers Opt. **61**, 223 (1995).
[5] V. Zehnlé, D. Dangoisse, and P. Glorieux, Opt. Commun. **90**, 99 (1992).
[6] G. Gouesbet *et al.*, Ann. N.Y. Acad. Sci. **808**, 25 (1996).
[7] T. Sauer, J.A. Yorke, and M. Casdagli, J. Stat. Phys. **65**, 579 (1991).
[8] J. Crutchfield and B. McNamara, Complex Syst. **1**, 417 (1987).
[9] M. Giona, F. Lentini, and V. Cimagalli, Phys. Rev. A **44**, 3496 (1991).
[10] M.V. Corrêa, A. Aguirre, and E.M.A.M. Mendes, Int. J. Bifurcation Chaos Appl. Sci. Eng. **10**, 1019 (2000).
[11] R. Hegger *et al.*, Chaos **8**, 727 (1998).
[12] J. Cremers and A. Hübler, Z. Naturforsch., A: Phys. Sci. **42**, 797 (1987).
[13] L. Jaeger and H. Kantz, Chaos **6**, 440 (1996).
[14] J. Timmer, Int. J. Bifurcation Chaos Appl. Sci. Eng. **8**, 1505 (1998).
[15] B. van Domselaar and P. W. Hemker, Math. Centre Amsterdam Technical Report No. NW 18/75 (unpublished).
[16] H.G. Bock, in *Numerical Treatment of Inverse Problems in Differential and Integral Equations*, edited by P. Deuflhard and E. Hairer (Birkhäuser, Basel, 1983), pp. 95–121.
[17] F. Meyer-Bourbonneux, J. Dupré, and C. Meyer, Can. J. Phys. **54**, 205 (1976).
[18] M. Ciofini and R. Meucci, IEEE J. Quantum Electron. **31**, 886 (1995).
[19] E. Hairer, S. P. Nørsett, and G. Wanner, *Solving Ordinary Differential Equations I* (Springer, Berlin, 1987).
[20] W. Horbelt, Ph.D. thesis, University of Freiburg, 2001, http://webber.physik.uni-freiburg.de/~horbelt/diss
[21] R. Meucci, M. Ciofini, and R. Abbate, Phys. Rev. E **53**, R5537 (1996).
[22] R. Meucci, P. Wang, and A. Lapucci, Opt. Lett. **16**, 1040 (1991).
[23] S. Balle *et al.*, Phys. Rev. Lett. **72**, 3510 (1994).
[24] H. Grassi *et al.*, Phys. Rev. A **50**, 805 (1994).
[25] F.T. Arecchi, W. Gadomski, R. Meucci, and J.A. Roversi, Phys. Rev. A **39**, 4004 (1989).
[26] D. Bromley *et al.*, Opt. Commun. **99**, 65 (1993).
[27] M. Ciofini, R. Meucci, and F.T. Arecchi, Phys. Rev. A **42**, 482 (1990).
[28] C.P. Christensen, C. Freed, and H.A. Haus, IEEE J. Quantum Electron. **5**, 276 (1969).